Stochastic Emergence of Irregular Infection Fronts in Motile Bacteria-Phage Populations

Laura Bergamaschi[1], Namiko Mitarai[1]

[1] *The Niels Bohr Institute, University of Copenhagen, Niels Bohr Bygningen, Jagtvej 128, Copenhagen N, 2200, Denmark*

October 29, 2025

Abstract

Interactions between bacteriophages and motile bacteria can produce irregular spatial patterns that deterministic models fail to capture. Here we show that these irregularities arise from stochastic infection dynamics at the single-cell level. We develop a discrete, stochastic model of phage–bacteria co-propagation, which represents bacteria and phages as non-negative integers on a two-dimensional lattice, while nutrients and attractants remain continuous fields. Stochastic rules govern bacterial growth, chemotactic movement, infection, and lysis, allowing spatial heterogeneity to emerge in agreement with experimentally observed asymmetric patterns. Simulations reveal that rare events, in which an infected bacterium migrates ahead of the front before lysis, locally seed new infection centers. The resulting front roughness is controlled by the product of burst size and adsorption rate, and is suppressed when the effective population size increases or the variability of latent period decreases. These results link microscopic stochasticity to emergent spatial structure in phage–bacteria populations.

1 Introduction

Bacteriophages play a central role in microbial ecosystems [1], from the human gut to oceans and soil [2]. While phage–bacteria interactions have been extensively studied in well-mixed liquid cultures [3, 4], spatial structure and bacterial motility can fundamentally alter infection outcomes, promoting coexistence and diversification [5, 6, 7, 8, 9, 10, 11, 12, 13, 14, 15]. In structured environments (such as semi-solid agar), motile bacteria create their own nutrient gradients and chemotactically migrate along them [16, 17, 18, 19]. Traveling-wave solutions combining growth and chemotaxis have been analytically characterized

[20], providing theoretical context for bacterial front propagation. These expanding fronts often outpace the spread of phages, introducing a new regime in which non-motile phages must essentially 'hitchhike' by infecting moving bacteria to avoid being left behind [21, 22, 23, 24]. Experimental studies of such co-propagating phage–bacteria populations have revealed complex spatiotemporal dynamics – for example, the formation of distinct bacterial and phage spread fronts, and lysis zones where bacteria are cleared by phage [21, 22, 23, 24]. Notably, several features of these relatively smooth and symmetric patterns have been captured by traditional continuous models using deterministic partial differential equations (PDE) [21, 22, 23, 24].

However, experiments also suggest that chance events and variability can upset these smooth patterns. In the study by Ping et al. (2020), co-cultures of chemotactic *E. coli* and bacteriophage $P1_{vir}$ in swimming agar sometimes developed irregular, rough-edged lysis patterns instead of smooth expanding rings [21]. These rough "killing fronts" occurred under intermediate phage concentrations and adsorption rates – conditions near a transition between phage falling behind vs. overtaking the bacteria. Ping et al. attributed the irregular fronts to small stochastic fluctuations in the initial inoculum. More generally, such irregularities highlight the potential importance of randomness. Even without large initial perturbations, rare events can arise – for instance, a single bacterium infected at the leading edge might swim ahead of the pack and then lyse, seeding a new pocket of phages farther out. This one infection can lead to a burst of local phage that initiates a new infection focus, distorting the overall pattern. In other words, an initially minor, random event can be amplified by feedback into a macroscale asymmetry. However, such effects are inherently difficult to capture with PDE-based models.

To address this gap, we develop a discrete stochastic model of phage–bacteria interactions on a two-dimensional lattice, incorporating chemotaxis and nutrient consumption. This approach bridges experimental observations and continuum theory by explicitly tracking population counts per lattice site, rather than treating densities as continuous fields. Although individual cell trajectories are not resolved, the event-based stochastic dynamics capture essential effects of demographic noise and population discreteness that deterministic formulations miss. With this framework, we explore how parameters such as infection efficiency and the effective local population size influence emerging spatial patterns. We show that rare, discrete infection events play a central role in generating and shaping spatial heterogeneity, providing a computational platform to investigate the role of stochasticity in phage–host co-propagation.

2 Model

2.1 Principles of rules in the model

We consider a 2-dimensional lattice of size $L \times L$, with each site having a linear size of Δx in the xy plane. We assume the depth of the system Δz is a constant

and each site is locally well-mixed in the volume $V_{site} = \Delta x^2 \Delta z$. For each lattice point (x, y), we consider the number of uninfected bacteria $H(x, y)$, the number of infected bacteria $I_j(x, y)$ at the infection stage j (with $j = 1, 2, \cdots, m$), the number of free phages $P(x, y)$ as discrete variables (non-negative integers), the nutrient concentration $n(x, y)$ and the chemoattractants concentrations $c_k(x, y)$ (with $k = 1, 2$, representing serine and aspartate, respectively [16]) as continuous variables. The principles of the simulation are strongly inspired by the PDE model by Ping *et al.* [21]. Below, we summarize the basic principles of the model. The algorithm and default parameter values are summarised respectively in the supplementary texts S1 and S4 and a schematic representation of the model is shown in Figure 1.

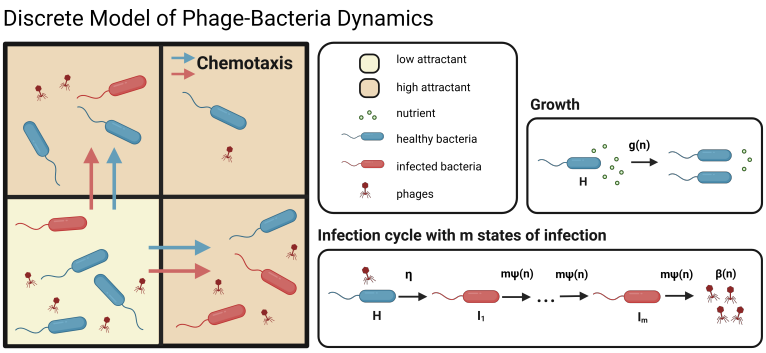

Figure 1: Schematic representation of the stochastic phage-bacteria model. Healthy bacteria grow by consuming nutrients and move via chemotaxis in response to attractant gradients. Phages infect bacteria, initiating a multi-step infection cycle with m states $(I_1, I_2, \ldots, I_m)$ that culminates in lysis and phage release. Created in BioRender. https://BioRender.com/c7eog9f

Bacterial Growth and Nutrient Dynamics: The dependence of the bacterial growth rate g on the local nutrient concentration $n(x, y)$ is modeled using the Monod growth law [25]:

$$g(n) = \frac{g_{\max}\, n}{K_n + n}, \tag{1}$$

where $g_{\max}$ represents a constant maximum growth rate, and K_n is the half-saturation constant. We interpret this as a stochastic division rate in the algorithm to let the number of healthy cells H increase over time. In each location, the nutrient is consumed by all bacteria $B(x, y) = H(x, y) + \sum_j I_j(x, y)$ with a consumption rate proportional to $g(x, y)$, with the yield coefficient Y. Chemoattractants are assumed to also be consumed and diffuse in a similar manner. If

all the field were continuous, they should obey

$$\frac{\partial n}{\partial t} = -\frac{1}{Y} \cdot g(n) \cdot B + D_n \left(\frac{\partial^2 n}{\partial x^2} + \frac{\partial^2 n}{\partial y^2} \right), \tag{2}$$

$$\frac{\partial c_i}{\partial t} = -\frac{1}{Y} \cdot \frac{g_{i,max}\, c_i}{K_i + c_i} \cdot B + D_n \left(\frac{\partial^2 c_i}{\partial x^2} + \frac{\partial^2 c_i}{\partial y^2} \right). \tag{3}$$

Here, D_n is the nutrient/chemoattractant diffusion constant, and $g_{i,max}$ and K_i are chemoattractant i's maximum consumption rate and Michaelis-Menten constant, respectively.

Diffusion and Chemotaxis: Phages are assumed to diffuse at a diffusion constant D_p, while bacteria moves diffusively due to run-and-tumble motion [26] with the diffusion constant D_b, when there is no chemoattractant gradient. In addition, when there is gradient in chemoattractants, bacteria (both healthy and infected) bias their movements according to the gradient of a log-ratio function of the chemoattractants

$$L_i(c_i) = \chi_i \log \left(\frac{1 + \frac{c_i}{a_-}}{1 + \frac{c_i}{a_+}} \right) \tag{4}$$

where χ_i is the chemotactic sensitivity for the i-th attractant, and a_- and a_+ are the saturation constants [16, 27]. These effects are implemented as stochastic redistribution of bacteria and phages in their neighbouring sites.

Infection and Lysis Dynamics: The infection is modeled by assuming that phages are able to adsorb to both healthy and infected bacteria, with the same adsorption rate η. This is implemented as stochastic events happening locally in each lattice site.
The latent period between adsorption and lysis is modeled by introducing m infection states of bacteria, I_j with $j = 1, 2, \cdots, m$, each with average lifetime of $\frac{1}{m\psi(n)}$, where $\psi(n)$ is the rate of lysis and depends on the nutrient concentration in the site with the following equation:

$$\psi(n) = \psi \left(r_l + (1 - r_l) \cdot \frac{g(n)}{g(n_0)} \right) \tag{5}$$

where ψ is the maximum lysis rate, r_l is the ratio of the maximum rate to the minimum rate, and n_0 is the initial nutrient concentration [21].
The cells in the infection state m will burst to produce phage progeny at the same rate $m\psi(n)$. The burst size of the lysing bacteria also depends on the nutrient concentration:

$$\beta(n) = \beta \left(r_b + (1 - r_b) \cdot \frac{g(n)}{g(n_0)} \right) \tag{6}$$

where β is the maximum burst size, and r_b is the ratio of the minimum burst size to its maximum [21].

These formulations capture the nutrient dependency such that lower host growth rates extend the latent period and reduce burst size. The inclusion of m sequential infection states approximates an Erlang distribution for the lysis time, rather than an exponential one, reducing the coefficient of variation of the latent period to $1/\sqrt{m}$. This is a standard technique in stochastic modelling to achieve a more realistic timing of biological processes [10, 28]. Progresses between the states are implemented stochastically with given rates.

2.2 Initial conditions, boundary conditions, and parameters

Parameters are estimated based on the experimentally known values [21] as described in Supplementary Section S5, and the default values are summarized in the Supplementary Table S1. We simulate the system under reflective boundary conditions. At time zero, $P(0)$ phages and $B(0)$ bacteria are placed in the left bottom corner lattice site, and nutrients and chemoattractants $n(0)$, $c_1(0)$, and $c_2(0)$ are uniformly distributed in all the lattice sites. This results in simulating 1/4 of the entire system.

3 Results

3.1 Emergence of spatio-temporal patterns

Using our discrete model that incorporates bacterial growth, nutrient and attractant diffusion and consumption, chemotactic migration, phage infection, and lysis (Figure 1; see Model section for details), we simulated pattern formation starting from a localized inoculum of bacteria and phages. A representative outcome with the default parameter set is shown in Figure 2. In this case, the number of infected states was set to $m = 2$, which produces a relatively broad distribution of latent periods with a high probability of short delays.

The simulations reproduced key experimental features. In the experiments of Ping et al. [21], the killing front advanced much faster than could be explained by free phage diffusion. To account for this, they proposed that infected bacteria remain motile and chemotactic, thereby transporting phages until lysis. We implemented this assumption in our discrete model, which likewise produced two distinct bacterial fronts driven by the two chemoattractants, together with a phage front that "hitchhiked" with migrating infected cells. Under the chosen parameter set, this coupling led to an increasingly irregular killing front with radial protrusions over time in our model (Figure 2, top panel).

The roughening of the front arose from stochastic infection events. As shown in the bottom panel of Figure 2, where $\log(\sum_j I_j(x, y))$ highlights infected sites, even a single infected bacterium at the leading edge could seed a new extension. If such a cell migrated sufficiently far before lysis, it initiated a new cluster of infections that enabled phages to keep pace with the expanding bacterial front.

In regions where no such rare events occurred, phages lagged behind and the infection front advanced more slowly.

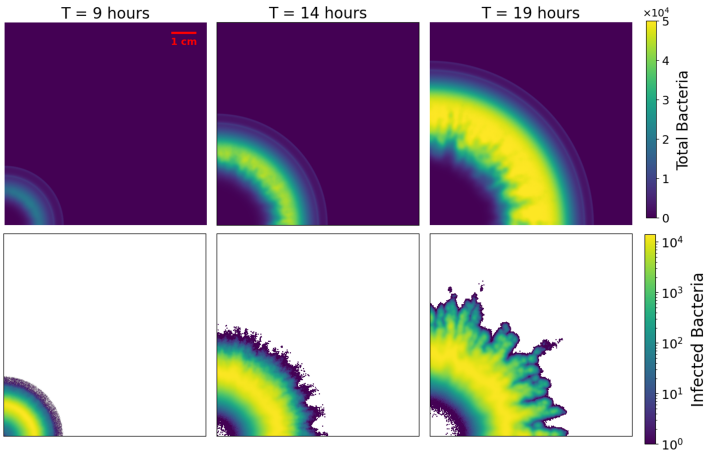

Figure 2: Spatio-temporal evolution of phage-bacteria dynamics. In the uppper panels we show total bacteria patterns after 9 h, 14 h, and 19 h, showing the formation of irregular killing fronts. In the lower panels we show the corresponding logarithmic counts of infected bacteria, highlighting stochastic seeding events at the advancing front. Simulations start with $\Delta z \times 10^4$ initial bacteria and the same amount of initial phages in the lower-left corner; depth $\Delta z = 5$ mm, $\beta = 20$ and $\eta = 1.5 \cdot 10^{-8}$ mL h^{-1}.

The emergent patterns depended strongly on the phage–bacteria interaction parameters. To probe how infection dynamics shapes these patterns, and in particular when stochastic roughening emerges, we systematically varied the adsorption rate (η) and burst size (β) across a broad range of values (Figure 3a). For small η and β, phage killing was weak: bacterial migration dominated, and phages were left behind, remaining only near the inoculation site. As η and β increased, the bacterial front became progressively suppressed, culminating in collapse of the migrating population. Stochastic, irregular patterns arose at intermediate values, where phage expansion and bacterial migration proceeded at comparable rates. In this regime, rare infection events determined whether phages successfully colonized new regions, underscoring the importance of discreteness in shaping spatial dynamics.

To quantify bacterial survival in these simulations, we calculated the average bacterial concentration at the end of each run (19 h after inoculation), defined as

$$\varrho = \sum_{(x,y)} \frac{B(x,y)}{V_{site} L^2}, \tag{7}$$

where $B(x,y)$ is the number of bacteria at lattice site (x,y), V_{site} is the site volume, and L^2 the total system area. The resulting values of ϱ are shown in

Figure 3b for each (η, β) pair. When plotted against the product $\eta \cdot \beta$, the results collapse onto a single curve, indicating that the combined efficiency of adsorption and phage production acts as a natural control parameter. To illustrate representative cases within the intermediate regime, we selected two parameter combinations (η, β) corresponding to distinct realizations of stochastic patterns, highlighted in red in Figure 3a. In Figure 3b a dashed line is drawn at the associated values of $\eta \cdot \beta$ to indicate their position within the parameter space. Both cases exhibit irregular, stochastic patterns, characteristic of this intermediate regime.

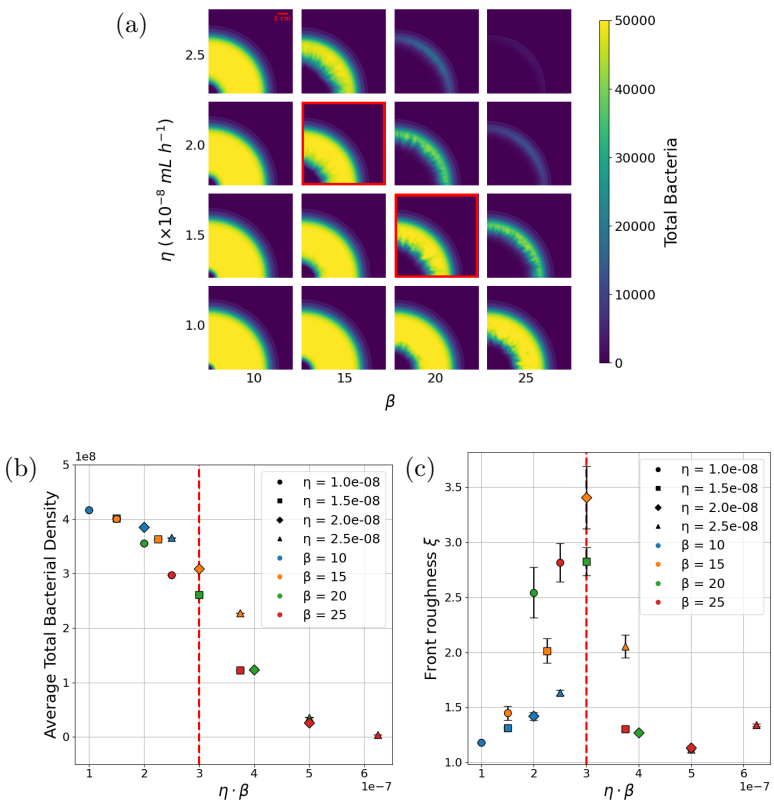

Figure 3: Dependence of spatial dynamics on phage–bacteria interaction parameters. (a) Phase diagram of final bacterial patterns for varying η and β. (b) Average total bacterial density ϱ after 19 h as a function of $\eta \cdot \beta$. (c) Frontier roughness ratio ξ as a function of $\eta \cdot \beta$. Each symbol represents the mean across $n = 3$ independent replicates, with error bars indicating the standard error of the mean. The dashed red lines mark the parameter combinations highlighted in panel (a). Simulations start with$\Delta z \cdot 10^4$ initial bacteria and the same amount of initial phages in the lower-left corner; $\Delta z = 5$ mm.

To be able to quantify this geometric effect and compare between different spatial patterns, we introduced a dimensionless front roughness measure:

$$\xi = \frac{P_{\text{infected}}}{P_{\text{qc}}} \tag{8}$$

defined as the ratio between the measured infection-front perimeter and that of a quarter-circle of equal infected area (see Supplementary Section S2 for details). The dependence of ξ on $\eta \cdot \beta$ is shown in Figure 3c. As expected, ξ peaks at intermediate values of $\eta \cdot \beta$, corresponding to the red-highlighted parameter combinations in Figure 3a. For small or large $\eta \cdot \beta$, ξ approaches unity, indicating smooth, circular fronts. In contrast, intermediate conditions yield elevated ξ values, reflecting the emergence of irregular and stochastic invasion dynamics.

3.2 The irregular pattern is due to the small number effect

To quantify the role of stochasticity, particularly rare events where a single infected bacterium migrates far ahead of the front, we simulated systems of varying depth Δz, under the assumption of well-mixed dynamics along the depth dimension. Initial conditions were scaled to maintain identical concentrations. Hence, increasing Δz effectively increased the number of individuals per lattice site while keeping the concentrations. In the limit $\Delta z \to \infty$, stochastic fluctuations due to finiteness of individuals is expected to vanish due to the law of large numbers.

Changing the effective number of individuals alters both the likelihood and the impact of rare events. Larger depths increase the chance that a single infected cell travels far for each location, but the effect of such an event becomes diluted because each burst affects a smaller fraction of the local population. This trade-off is evident in Figure 4. As shown in Figure 4a, greater depths produce more radial "spikes" in the phage front, but the spikes appear with weaker contrast, yielding smoother phage fronts and more uniform bacterial distributions overall. The dependence of the front roughness ξ on Δz is shown in Figure 4b: systems with lower depth exhibit higher ξ values, indicating rougher, more irregular fronts, while increasing Δz leads to smoother, more circular colonies, characterized by lower values of ξ. The first point at $\Delta z = 0.2$ mm is less representative due to the nature of the front-roughness measure, which penalizes fronts with fewer spikes.

This trend is further quantified in Figure 4c, which shows radial averages, and in Figure 4d which shows standard deviations of bacterial densities. At larger depths, the radial profiles become smoother and the standard deviations decrease, indicating reduced spatial heterogeneity. Separately, we simulated the deterministic partial differential equation (PDE) version of the model in 2-dimension, and we confirmed it shows no instability of the killing front (Supplementary Material S3). However, the ensemble average at large depth does not lie closer to the PDE curve for larger Δz within the range we could simulate: at small depths, rare runner events are infrequent, so the mean is often

dominated by typical 'no-runner' realizations and can appear closer to the PDE. At large depths, runner events become common but individually weaker, which lowers variability yet can bias the mean front outward. We could not simulate much larger Δz due to the high computational cost, hence we could not confirm or disconfirm if the system eventually converge to PDE result in $\Delta z \to \infty$ limit.

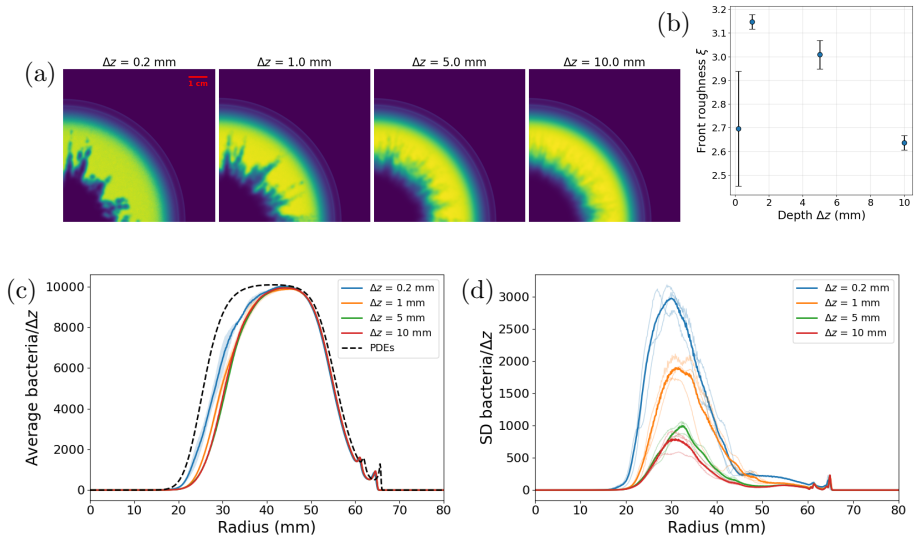

Figure 4: Impact of system depth on phage–bacteria infection dynamics. (a) Final patterns at 19 hours for simulations with different depths: $\Delta z \cdot 10^4$ initial bacteria and the same amount of initial phages in site $(0, 0)$. Simulations use $\beta = 20$ and $\eta = 1.5 \cdot 10^{-8}$ mL h^{-1} (In the DM $\eta = 3.0 \cdot 10^{-4}$ h^{-1}). (b) Frontier roughness ratio ξ as a function of Δz. Each point shows the mean $\pm$ standard error of the mean across $n = 3$ independent replicates. (c) Radial average profiles (radius in mm) for each depth (Δz). Curves show the mean across n=3 independent replicates, with shaded bands indicating the standard error of the mean across replicates. To enable comparison across depths, the mean is normalized by Δz (y-axis: Average bacteria/Δz). A dashed black curve shows the corresponding PDE result for reference. (d) Radial standard-deviation profiles. Thin lines indicate individual replicate standard deviation profiles, and bold lines show the pooled standard deviation (square root of the mean of replicate variances). Values are normalized by Δz (y-axis: Std bacteria/Δz).

3.3 Effects of latent period length distribution on infection front stochasticity

The results so far indicate that irregular front roughening originates from the amplification of rare events where a single infected bacterium lyses ahead of the

average front. For such an event to produce a visible clearing, the initial burst must be amplified by successive rounds of infection. This process may couple two extremes of the latent period distribution: a bacterium with a relatively long latent period can carry phages far ahead before bursting, while progeny from a bacterium with a short latent period can rapidly initiate secondary infections. Consequently, the distribution of latent periods is expected to strongly influence the emergent patterns.

To test this, we varied the number of discrete infected states m, which generates an Erlang distribution of latent period length with coefficient of variation CV $= 1/\sqrt{m}$. When $m = 1$, lysis times follow an exponential distribution (CV $= 1$), leading to highly irregular fronts with broad, dark spikes (Figure 5, leftmost panel). As m increases, the latent period distribution becomes more sharply peaked around the mean. This reduction in variance suppresses extreme outliers and diminishes the large-scale roughening of the front. Panels for $m = 2$ and $m = 3$ show progressively thinner, less pronounced spikes, and by $m = 5$ the infection front appears smooth and uniform.

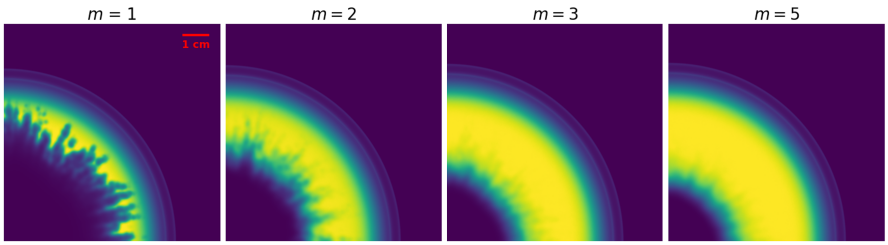

Figure 5: Effect of lysis time distribution on spatial infection patterns. Infection patterns after 19 h for Erlang distributions with $m = 1, 2, 3, 5$ substeps (coefficient of variation CV $= 1 \,/\, \sqrt{m}$). As m increases, the phage spread decreases and the infection front becomes smoother. All simulations use $\beta = 20$ and $\eta = 1.5 \cdot 10^{-8}$ mL h^{-1}.

We further tested whether adsorption kinetics could compensate for this effect. As shown in Figure S4, increasing η at $m = 5$ did not restore the thick, irregular spikes characteristic of the low-m regime. Taken together, these results indicate that the shape of the latent period distribution—not just the mean latent time or adsorption rate—critically determines macroscopic pattern variability. Exponential lysis amplifies demographic noise and produces rough, irregular fronts, whereas multi-step Erlang distributions concentrate lysis events near the mean, suppressing outliers and yielding smoother, more deterministic fronts.

As we stated before, increasing the parameter m effectively narrows the distribution of latent periods. However, it remains unclear whether the shorter or longer latent periods are primarily responsible for the emergence of irregular pattern. To address this, we constructed a modified model (presented in more detail in Supplementary Section S4) in which, upon infection, each cell is stochastically assigned to one of several latency-time distributions. In 90% of

cases, cells follow the Erlang distribution with $m = 3$ and a mean latency of 1 hour, while the remaining 10% are assigned to a Erlang distribution with $m = 3$ and a mean latency of either 3 hours or 20 minutes, depending on the simulation. The obtained distributions are shown in Figure 6a with the Erlang distribution of $m = 3$. This approach allows us to disentangle the respective contributions of short and long latent periods to the overall population dynamics. The results, presented in Figure 6b, show that rare early lysis events are more effective at restoring roughness than late outliers, highlighting the asymmetric role of the distribution tails in shaping front geometry. A similar asymmetry arises when considering heterogeneity in motility (Supplementary Section S4): less responsive cells have little effect, whereas a minority of more motile infected cells can travel further up the gradient and lyse ahead of the front, again generating forward outliers that restore roughness.

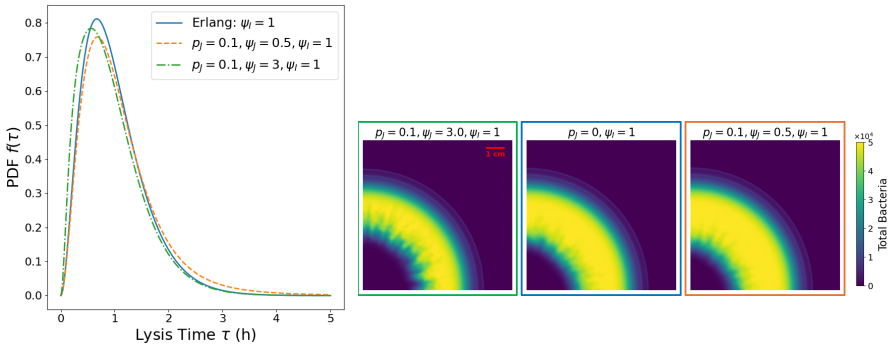

(a) (b)

Figure 6: Impact of faster or slower lysing subpopulations on infection front structure.(a) Probability density functions of lysis time for an Erlang distribution ($\psi = 1$, blue) and mixtures with a minority subpopulation, having either slower lysis $\psi_J = 0.5$, orange dashed) or faster lysis ($\psi_J = 3$, green dash-dotted). (b) Spatial infection fronts under mixed lysis rates: snapshots of total bacterial density for three parameter sets: (left) minority fast-lysing infections ($p_J = 0.1, \psi_J = 3, \psi_I = 1$); (center) baseline Erlang distribution ($p_J = 0, \psi_I = 1$); (right) minority slow-lysing infections ($p_J = 0.1, \psi_J = 0.5, \psi_I = 1$). Rough fronts are restored when early lysis events are present (left), while late outliers (right) do not have a strong effect on the shape of the front.

4 Discussion

We developed a discrete model that successfully reproduces the irregular spatial patterns observed in experimental studies of interaction between phage and motile bacteria, capturing key features that are inaccessible by deterministic PDE approaches. By explicitly modelling discrete events in phage-bacteria interactions and incorporating stochasticity, the model reveals how spatial heterogeneity naturally emerges from the interplay between bacterial migration and phage infection. In particular, we show that rare infection events, such as a single infected bacterium migrating ahead of the front before lysis, can generate new centers of infection, having a strong effect on large-scale dynamics. This sensitivity to individual events underscores the importance of treating infection and transport as discrete processes.

Our results further identify the product of adsorption rate and burst size ($\eta \cdot \beta$) as a critical control parameter governing population outcomes. A transition from bacterial survival to extinction emerges as $\eta \cdot \beta$ increases, reflecting a trade-off between phage reproductive efficiency and bacterial dispersal. This theoretical prediction is consistent with the experiments of by Ping *et al.* [21]where modulation of the phage $\mathrm{P1_{vir}}$ adsorption rate via calcium concentration produced analogous shifts in the observed pattern.

Moreover, we demonstrate that increasing the depth of the lattice, which effectively increases the number of individuals per site, suppresses the impact of stochastic fluctuations and leads the system toward a smooth killing pattern. This suggests that population size and demographic noise fundamentally shape infection front dynamics, with implications for understanding pattern formation in natural microbial communities.

Finally, by varying the number of discrete infected states, we show that the shape of the latent period distribution itself—not just its mean—critically modulates front roughness. We demonstrated that the occasional burst with short latent time is particularly important for the irregular killing patterns, likely due to exponential amplification of phage following after such an event. This is an experimentally testable prediction if one can identify phage mutants that have different latent period distribution. The impact of latent period distribution has been recently highlighted in several theoretical works [29, 30]. This indicates the importance of characterizing the latent time distributions experimentally, which is becoming feasible thanks to the recent development of single cell measurements [31].

We have also found that having subpopulation of infected cell that swim faster than others could also be a possible way to have irregular pattern. It should be noted that the infection itself is more likely to reduce bacterial motility by interfering with cellular physiology; however, a similar effect is expected to arise if the bacterial population already exhibits heterogeneity in chemotactic ability prior to infection. It should also be noted that, even though some degree of swimming of infected bacteria is widely accepted based on the experimentally observed pattern [21, 22, 24], a recent single-cell experiment showed infection by λ phage can diminish the ability of *E. coli* flagella motor to rotate [32].

Furthermore, a previous study has reported that phages can be transported by non-host motile bacteria [33], suggesting that transport by uninfected cells may also play an important role. Characterizing attachment of phage to swimming bacteria and the ability of infected cells to swim at single-cell level would also be an important experimental step to fully understand the observed killing patterns.

The model has several limitations. Although it incorporates stochasticity and discrete population counts, it does not track individual cell trajectories or infection histories. This limits the ability to model processes that depend on cell-level timing or movement histories. Another limitation is that all bacteria are assumed to have identical chemotactic and motility parameters. In reality, mutations or phenotypic variability can lead to subpopulations with distinct swimming speeds or chemotactic responses [34, 35, 36], potentially altering infection dynamics and spatial pattern formation. Additionally, all bacteria are assumed to be susceptible to infection. In natural systems, spontaneous mutations can lead to resistance or altered infection phenotypes, which are crucial for long-term coexistence and evolution[37, 38]. It is left for future work to address the effect of mutations in observed patterns.

Our model connects single-cell stochasticity with population-scale organization, highlighting how fluctuations at the microscopic level can determine macroscopic outcomes. This insight may extend beyond phage–bacteria dynamics to other systems in which growth and dispersal are coupled, such as microbial range expansions, ecological invasions, or viral epidemics. More generally, our findings emphasize the need to consider demographic fluctuations not as noise to be averaged out, but as an intrinsic driver of spatial pattern formation in living systems.

Code Availability

The source code will be made available at:`https://github.com/laurabergamaschi22/phage_motile_bacteria_model_code.git`

Acknowledgement

This research was funded by the Novo Nordisk Foundation (NNF21OC0068775).

References

[1] E. Kutter and A. Sulakvelidze. *Bacteriophages: Biology and Applications*. CRC Press, Boca Raton, FL, 2005.

[2] Anne Chevallereau, Benoît J. Pons, Stineke van Houte, and Edze R. Westra. Interactions between bacterial and phage communities in natural environments. *Nature Reviews Microbiology*, 20(1):49–62, 2022.

[3] B. J. Bohannan and R. E. Lenski. Effect of resource enrichment on a chemostat community of bacteria and bacteriophage. *Ecology*, 78:2303–2315, 1997.

[4] B. R. Levin, F. M. Stewart, and L. Chao. Resource-limited growth, competition, and predation: a model and experimental studies with bacteria and bacteriophage. *American Naturalist*, 111:3–24, 1977.

[5] Benjamin Kerr, Margaret A. Riley, Marcus W. Feldman, and Brendan J. M. Bohannan. Local dispersal promotes biodiversity in a real-life game of rock–paper–scissors. *Nature*, 418:171–174, 2002.

[6] Benjamin Kerr, Claudia Neuhauser, Brendan J. M. Bohannan, and Antony M. Dean. Local migration promotes competitive restraint in a host–pathogen "tragedy of the commons". *Nature*, 442:75–78, 2006.

[7] Wei Wei and Stephen M. Krone. Spatial invasion by a mutant pathogen. *Journal of Theoretical Biology*, 236:335–348, 2005.

[8] S. Heilmann, K. Sneppen, and S. Krishna. Coexistence of phage and bacteria on the boundary of self-organized refuges. *PNAS*, 109:12828, 2012.

[9] Ben Ashby, Sunetra Gupta, and Angus Buckling. Spatial structure mitigates fitness costs in host–parasite coevolution. *The American Naturalist*, 183(1):E64–E74, 2014.

[10] N. Mitarai, S. Brown, and K. Sneppen. Population dynamics of phage and bacteria in spatially structured habitats using phage λ and escherichia coli. *Journal of Bacteriology*, 198(12):1783–1793, 2016.

[11] James J. Bull, Christoffer S. Vegge, Matthew Schmerer, Waqas N. Chaudhry, and Bruce R. Levin. Phage–bacterial dynamics with spatial structure: self-organization around phage sinks can promote increased cell densities. *Antibiotics*, 7(1):8, 2018.

[12] R. S. Eriksen, N. Mitarai, and K. Sneppen. Sustainability of spatially distributed bacteria-phage systems. *Scientific Reports*, 10:3154, 2020.

[13] Emily L. Simmons, Megan C. Bond, Knut Drescher, Carey D. Nadell, Vanni Bucci, and Bonnie L. Bassler. Biofilm structure promotes coexistence of phage-resistant and phage-susceptible bacteria. *mSystems*, 5(3):e00877–19, 2020.

[14] R. S. Eriksen, F. Larsen, S. L. Svenningsen, K. Sneppen, and N. Mitarai. The dynamics of phage predation on a microcolony. *Biophysical Journal*, 123:147, 2024.

[15] A. Yadav, N. Mitarai, and K. Sneppen. Self-organized coexistence of phage and a population of host colonies. *bioRxiv*, 2024.

[16] J. Cremer, T. Honda, Y. Tang, J. Wong-Ng, M. Vergassola, and T. Hwa. Chemotaxis as a navigation strategy to boost range expansion. *Nature*, 575:658–663, 2019.

[17] H. C. Berg and D. A. Brown. Chemotaxis in escherichia coli analysed by three-dimensional tracking. *Nature*, 239(5374):500–504, October 1972.

[18] M. J. Schnitzer. Theory of continuum random walks and application to chemotaxis. *Physical Review E*, 48(4):2553, 1992.

[19] T. Jakuszeit, J. Lindsey-Jones, F. J. Peaudecerf, and O. A. Croze. Migration and accumulation of bacteria with chemotaxis and chemokinesis. *The European Physical Journal E*, 44(3):32, 2021.

[20] Avaneesh V. Narla, Jonas Cremer, and Terence Hwa. A traveling-wave solution for bacterial chemotaxis with growth. *Proceedings of the National Academy of Sciences of the United States of America*, 118(48):e2105138118, 2021.

[21] D. Ping, T. Wang, D. T. Fraebel, S. Maslov, K. Sneppen, and S. Kuehn. Hitchhiking, collapse, and contingency in phage infections of migrating bacterial populations. *The ISME Journal*, 14(8):2007–2018, May 2020.

[22] X. Li, F. Gonzalez, N. Esteves, B.E. Scharf, and J. Chen. Formation of phage lysis patterns and implications on co-propagation of phages and motile host bacteria. *PLoS Comput Biol*, 16(3):e1007236, 2020.

[23] Yi Zhang, Qingjuan Hu, Yingtong Su, Pan Chu, Ting Wei, Xuefei Li, Chenli Liu, and Xiongfei Fu. Navigated range expansion promotes migratory culling. *Proceedings of the National Academy of Sciences*, 121(50):e2408303121, 2024.

[24] Jacopo Marchi, Chadiga Khalek, Abir George, Joshua S Weitz, and Remy Chait. Stable coexistence and transport of lytic phage infections with migrating bacterial hosts. *bioRxiv*, pages 2025–04, 2025.

[25] Jacques Monod. The growth of bacterial cultures. *Annual Review of Microbiology*, 3(1):371–394, 1949.

[26] J. Tailleur and M. E. Cates. Statistical mechanics of interacting run-and-tumble bacteria. *Physical Review Letters*, 100(21):218103, May 2008.

[27] Yuhai Tu, Thomas S. Shimizu, and Howard C. Berg. Modeling the chemotactic response of Escherichia coli to time-varying stimuli. *Proceedings of the National Academy of Sciences*, 105(39):14855–14860, 2008.

[28] Willem de Graaf, Laura Ernest, and Donald Ludwig. Discrete stochastic analogs of erlang epidemic models. *Journal of Biological Dynamics*, 14(1):78–96, 2020.

[29] Marian Dominguez-Mirazo, Jeremy D Harris, David Demory, and Joshua S Weitz. Accounting for cellular-level variation in lysis: implications for virus–host dynamics. *Mbio*, 15(8):e01376–24, 2024.

[30] Aaron Smith, Michael Hunter, Somenath Bakshi, and Diana Fusco. Live and let die: lysis time variability and resource limitation shape lytic bacteriophage fitness. *bioRxiv*, pages 2025–07, 2025.

[31] Charlie Wedd, Temur Yunusov, Aaron Smith, Ruizhe Li, Georgeos Hardo, Michael Hunter, Racha Majed, Diana Fusco, and Somenath Bakshi. Single-cell imaging of the lytic phage life cycle in bacteria. *bioRxiv*, pages 2024–04, 2024.

[32] Thu Vu Phuc Nguyen, Yuchen Wu, Tianyou Yao, Jimmy T Trinh, Lanying Zeng, Yann R Chemla, and Ido Golding. Coinfecting phages impede each other's entry into the cell. *Current Biology*, 34(13):2841–2853, 2024.

[33] Xin You, René Kallies, Ingolf Kühn, Matthias Schmidt, Hauke Harms, Antonis Chatzinotas, and Lukas Y Wick. Phage co-transport with hyphal-riding bacteria fuels bacterial invasion in a water-unsaturated microbial model system. *The ISME Journal*, 16(5):1275–1283, 2022.

[34] David T. Fraebel, Harry Mickalide, Diane Schnitkey, Jason Merritt, Thomas E. Kuhlman, and Seppe Kuehn. Environment determines evolutionary trajectory in a constrained phenotypic space. *eLife*, 6:e24669, 2017.

[35] X. Fu et al. Spatial self-organization resolves conflicts between individuality and collective migration. *Nature Communications*, 9:2177, 2018.

[36] J. Partridge, N. Nhu, Y. Dufour, and R. Harshey. Escherichia coli remodels the chemotaxis pathway for swarming. *mBio*, 10, 03 2019.

[37] G. H. Beale. A method for the measurement of mutation rate from phage sensitivity to phage resistance in escherichia coli. *Microbiology Society*, 2(2):131, 1948.

[38] S. E. Tamar and R. Kishony. Multistep diversification in spatiotemporal bacterial-phage coevolution. *Nature Communications*, 13:7971, 2022.